ISSN 0020-1685, Inorganic Materials, 2020, Vol. 56, No. 1, pp. 14–19. © Pleiades Publishing, Ltd., 2020.
Russian Text © The Author(s), 2020, published in Neorganicheskie Materialy, 2020, Vol. 56, No. 1, pp. 16–21.

Crystallization Behavior and Resistivity of Al–Ni–Co–Nd(Sm) Amorphous Alloys[1]

B. A. Rusanov[a, *], V. E. Sidorov[a, b], P. Svec[c], P. Svec, Sr.[c], D. Janickovic[c], and S. A. Petrova[b, d]

[a] *Ural State Pedagogical University, pr. Kosmonavtov 26, Yekaterinburg, 620017 Russia*
[b] *Ural Federal University, ul. Mira 19, Yekaterinburg, 620002 Russia*
[c] *Institute of Physics, Slovak Academy of Sciences, Dúbravská cesta 9, Bratislava, 84511 Slovakia*
[d] *Institute of Metallurgy, Ural Branch, Russian Academy of Sciences, ul. Amundsena 101, Yekaterinburg, 620016 Russia*
**e-mail: rusfive@mail.ru*

Received December 16, 2018; revised June 4, 2019; accepted June 6, 2019

Abstract—Aluminum-based metallic ribbons with the compositions $Al_{86}Ni_4Co_4Nd(Sm)_6$ and $Al_{86}Ni_6Co_2Nd(Sm)_6$ were produced by melt spinning. X-ray diffraction characterization showed that the ribbons had an amorphous structure. Their crystallization kinetics were studied by differential scanning calorimetry and their resistivity was measured by a standard four probe method. The Al–Ni–Co–REM ribbons were shown to have a broader temperature range of an amorphous state than do Al–Ni(Co)–REM ternary alloys. We found compositions with an enhanced glass-forming ability.

Keywords: aluminum alloys, amorphous ribbons, crystallization, structure, differential scanning calorimetry, resistivity

DOI: 10.1134/S0020168519120112

INTRODUCTION

Aluminum-based amorphous ribbons containing transition metals (TM = Ni or Co) and rare-earth metals (REMs) offer a unique combination of mechanical properties and corrosion resistance [1–5]. If nickel is used as a transition metal, the amorphous alloys possess improved mechanical properties (their tensile strength reaching 1000 MPa) [1]. At the same time, cobalt-containing ribbons demonstrate high corrosion resistance [6]. It is reasonable to expect that combining these elements in amorphous Al–Ni–Co–REM alloys will ensure the formation of metallic glasses with improved mechanical properties and corrosion resistance.

The purpose of this work is to study how the presence of Nd and Sm and the content of 3*d* transition metals influence glass formation in Al–Ni–Co–REM alloys (containing 4–6 at % Ni, 2–4 at % Co, and 6 at % Nd or Sm) and their electrical properties.

EXPERIMENTAL

Alloys for amorphous ribbons were prepared by melting starting materials in an induction furnace at 1923 K over a period of 0.5 h under an argon atmosphere. The chemical composition of the alloys was determined on an atomic absorption spectrometer. Amorphous ribbons (2 mm in width and 36–45 μm in thickness) with the compositions $Al_{86}Ni_4Co_4Nd_6$, $Al_{86}Ni_6Co_2Nd_6$, $Al_{86}Ni_4Co_4Sm_6$, and $Al_{86}Ni_6Co_2Sm_6$ were produced by melt spinning under a controlled inert gas atmosphere. First, we evacuated air from the chamber, and then it was filled with argon to a pressure of 10^3 Pa. The melt was superheated to 1500–1523 K in the induction furnace and then jetted onto a water-cooled copper drum.

The structure of the resultant samples was studied by X-ray diffraction (CuK_α radiation) on a Bruker D8 Advance diffractometer. They were characterized by differential scanning calorimetry (DSC) at heating rates of 10, 20, and 40 K/min using a PerkinElmer DSC-7 system. The resistivity of the ribbons was measured by the four probe method at a heating rate of 10 K/min. The experimental procedure was described in detail elsewhere [7].

RESULTS AND DISCUSSION

According to X-ray diffraction data, the ribbons had an amorphous structure (Fig. 1): no Bragg peaks were detected in their X-ray diffraction patterns. The main peak of the $Al_{86}Ni_4Co_4Nd_6$ and $Al_{86}Ni_6Co_2Nd_6$ ribbons is located at $2\theta = 38°–39°$, that is, at a 10°

[1] Presented at the 16th International IUPAC Conference on High Temperature Materials Chemistry (HTMC-XVI), July 2–6, 2018, Yekaterinburg, Russia.

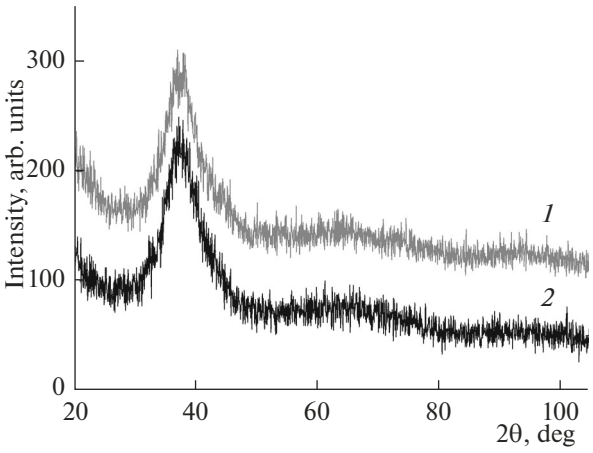

Fig. 1. X-ray diffraction patterns of the amorphous (*1*) $Al_{86}Ni_6Co_2Nd_6$ and (*2*) $Al_{86}Ni_4Co_4Nd_6$ ribbons (scan *1* is displaced upward by 100 units).

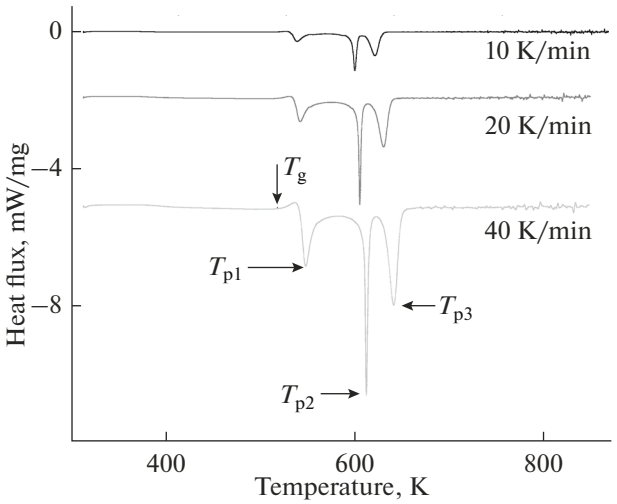

Fig. 2. DSC curves of the $Al_{86}Ni_6Co_2Nd_6$ alloy. The curves obtained at heating rates of 20 and 40 K/min are displaced downward by two and five units, respectively.

smaller angle in comparison with a ribbon containing 8 at % Ni [8]. The prepeak located to the left of the main peak and characteristic of nickel-containing ribbons [8] is shifted by a small angle. No such peak was detected in our experiments. The presence of Sm instead of Nd has no effect on the position of the main peak, but its intensity is higher by 50 units in the case of the neodymium-containing ribbons.

Figures 2 and 3 show typical DSC curves obtained at different heating rates.

All of the alloys were shown to have three exothermic peaks. In addition, the $Al_{86}Ni_6Co_2Sm_6$ alloy was found to have a fourth exothermic peak, with a small heat effect. The presence of Sm instead of Nd, at different relative amounts of the 3*d* transition metals, reduces not only the temperature of the first stage of crystallization (by 15–20 K) bur also the corresponding heat effect.

Table 1 lists the temperatures of the observed peaks in the DSC curves of the alloys.

Increasing the nickel content of the neodymium-containing ribbons to 6 at % was shown to reduce the temperatures of all three stages of crystallization. The temperatures of the first and second peaks were lower by 30 K, and that of the third peak decreased by 23 K. In addition, the heat effect of the first stage was smaller than that in the case of the alloy containing 4% Ni, whereas the heat effects of the second and third stages were larger. The third peak of these ribbons had a simple shape. Moreover, the glass transition in the $Al_{86}Ni_6Co_2Nd_6$ ribbons was only detected at high heating rates (20–40 K/min), in contrast to the $Al_{86}Ni_4Co_4Nd_6$ ribbons.

The results obtained for the alloys containing 6 at % Ni and 2 at % Co differ significantly for the neodymium- and samarium-containing ribbons. In addition to the fact that no glass transition was detected in the samarium-containing material, the first stage of its crystallization was shifted to lower temperatures by almost 46 K (at a heating rate of 10 K/min). Moreover, the heat effect in the first stage of crystallization decreases by almost three times. At the same time, these ribbons are similar in the nature of the second stage of crystallization (its temperature is 11 K higher in the case of the samarium-containing material). The peak temperature of the third stage of crystallization in the samarium-containing ribbons is higher than in the neodymium-containing ribbons (at any heating rate). It should be especially emphasized that, in this case, the heat effect in the samarium-containing material is considerably larger. In addition, at all heating rates the $Al_{86}Ni_6Co_2Sm_6$ alloy was found to have a fourth peak, at temperatures near 730 K, in contrast to the other samples. It seems likely that not only does a combination of 6 at % Ni, 2 at % Co, and 6 at % Sm considerably decrease the thermal stability of the amorphous state of the alloy, but it also stimulates an additional stage of crystallization.

At all heating rates, the glass transition temperature (T_g) is well-defined for the Nd-containing materials, which is atypical of amorphous aluminum-based alloys. The glass transition of the Sm-containing alloy with 4% Ni + 4% Co was only detected at high heating rates (20–40 K/min). This result correlates with previously reported DSC data for samarium-containing ternary alloys, whose T_g was never determined at a heating rate of 10 K/min [9–14].

The activation energy (E_p) for each stage of crystallization was evaluated by the Kissinger method [15], according to which

$$\ln\left(T_p^2/v\right) = E_p/RT_p + \text{const},$$

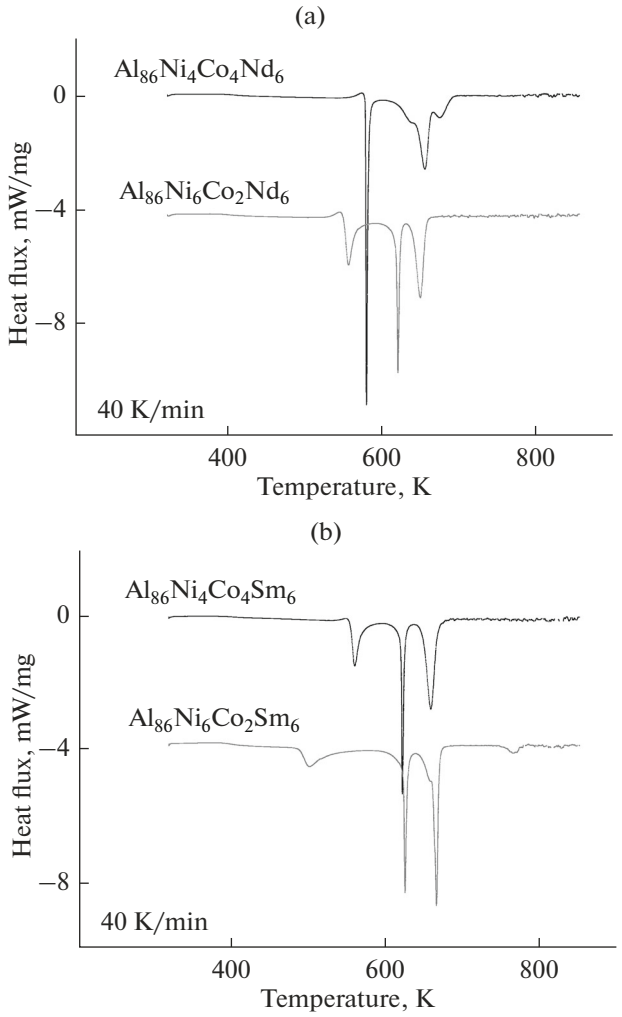

Fig. 3. DSC curves of the (a) Nd- and (b) Sm-containing alloys at a heating rate of 40 K/min. The curves of $Al_{86}Ni_6Co_2Nd_6$ and $Al_{86}Ni_6Co_2Sm_6$ are displaced downward by four units.

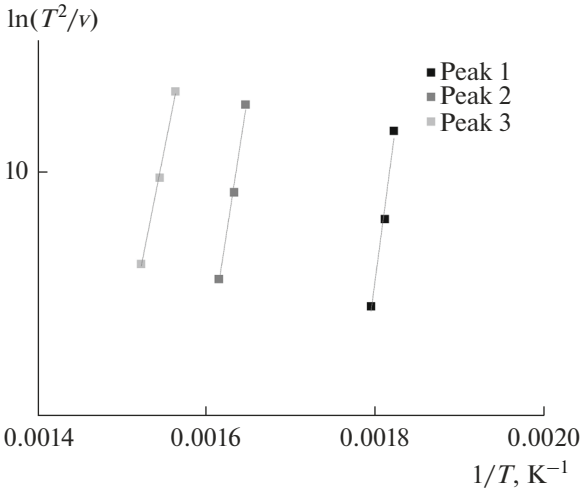

Fig. 4. Plots of $\ln(T^2/v)$ against $1/T$ for the $Al_{86}Ni_4Co_4Sm_6$ alloy.

where T_p is the peak temperature, v is the heating rate, and R is the gas constant.

The calculation results are presented in Fig. 4 and Table 2.

The activation energy was determined to be E_1 = 439 kJ/mol for the first stage of crystallization in the $Al_{86}Ni_4Co_4Nd_6$ alloy, E_2 = 240 kJ/mol for the second stage, and E_3 = 208 kJ/mol for the third stage. Replacing Nd by Sm increases E_1 to 408 kJ/mol. The activation energy increases by more than 100 kJ/mol for the second stage of crystallization and by more than 60 kJ/mol for the third stage. The addition of cobalt as a second transition metal considerably increases the activation energies for the first and second stages of crystallization in comparison with the values obtained by Illekova et al. [10] for an $Al_{89}Ni_6Sm_5$ ternary alloy.

Reducing the amount of Co from 4 to 2 at % reduces the activation energy for the first stage of crystallization to 353 kJ/mol, but increases the activation energies for the second and third stages to 339 and 216 kJ/mol, respectively.

Increasing the percentage of nickel in the samarium-containing alloys reduces the activation energy for the first stage of crystallization by almost a factor of 1.5, but raises the activation energy for the second stage of crystallization to 454 kJ/mol. The activation energy for the third stage of crystallization drops by 40 kJ/mol. The activation energy for the samarium-containing alloy with 6 at % Ni and 2 at % Co is substantially lower (by more than 90 kJ/mol for the first stage of crystallization) than that for the neodymium-containing alloy.

To identify the phases forming in different stages of crystallization, the ribbons were annealed for a short time, following which their structure was examined by X-ray diffraction. The ribbons were annealed during continuous heating at a rate of 10 K/min, followed by rapid cooling. The highest annealing temperatures were determined from the DSC results and corresponded to the first, second, and third peaks in the DSC curves of the alloys. The X-ray diffraction results for the $Al_{86}Ni_6Co_2Sm_6$ sample are presented in Fig. 5.

Pure aluminum was found to precipitate in the first stage of crystallization of the $Al_{86}Ni_6Co_2Sm_6$ alloy (Fig. 5, 570-K scan). The large width of the observed peaks in both the diffraction pattern and DSC curve of this sample suggests that aluminum precipitated in the form of nanoparticles. We observed the formation of the intermetallic phase Al_9Co_2 in the second stage of crystallization and the metastable compound Al_4Sm (or possibly $Al_{11}Sm_3$ with a distorted lattice) in the third stage. At a temperature near 738 K, the metastable intermetallic phase Al_4Sm converted into Al_3Sm, a

Table 1. Temperatures of the crystallization peaks in the DSC curves of the amorphous Al–Ni–Co–Nd(Sm) alloys

Composition	Heating rate, K/min	T_g, K	T_{p1}, K	T_{p2}, K	T_{p3}, K	T_{p4}, K
$Al_{86}Ni_4Co_4Nd_6$	10	540.7	563.6	628.9	644.3	–
	20	542.5	566.9	637.4	654.1	–
	40	544.2	571.8	647.7	666.8	–
$Al_{86}Ni_4Co_4Sm_6$	10	–	546.9	605.6	637.8	–
	20	524.1	550.6	610.5	645.3	–
	40	529.7	555.4	617.5	654.7	–
$Al_{86}Ni_6Co_2Nd_6$	10	–	539.3	600.5	621.7	–
	20	514.5	542.7	605.7	630.9	–
	40	515.4	548.7	612.6	641.6	–
$Al_{86}Ni_6Co_2Sm_6$	10	–	482.9	611.8	642.5	737.4
	20	–	490.4	614.8	653.7	748.5
	40	–	495.8	620.9	661.9	761.2

stable compound with a rhombohedral lattice (Fig. 5, 773-K scan).

On the whole, the $Al_{86}Ni_4Co_4Sm_6$ alloy exhibits similar crystallization behavior, but there are some distinctive features. First, the precipitation of aluminum nanoparticles in the first stage of crystallization begins at a 60-K lower temperature in comparison with the $Al_{86}Ni_6Co_2Sm_6$ alloy. Second, in the third stage the stable intermetallic phase Al_3Sm with a cubic lattice is formed at once. Subsequent heating of the material is not accompanied by any heat effects. After heating to 700 K and cooling to room temperature, the material consisted of Al, Al_9Co_2, and cubic Al_3Sm.

The X-ray diffraction results for the $Al_{86}Ni_4Co_4Nd_6$ alloy are presented in Fig. 6. Like in the case of the samarium-containing alloy, essentially pure aluminum precipitates in this alloy in the first stage of crystallization. Judging from the shape of the peaks in the X-ray diffraction pattern and DSC curve of this alloy, the pure aluminum particles in it are considerably larger than the aluminum nanoparticles precipitating in the samarium-containing alloys. In the second and third stages, the stable intermetallic compounds Al_9Co_2, Al_5Co_2, and Al_3Nd are formed, persisting to room temperature. It is worth noting that, after heating to 700 K, we observed reflections corresponding to the $AlNd_3$ compound, even though the existence of this compound at 6% neodymium appears unlikely. It is quite possible that there was a small amount of a ternary compound whose X-ray diffraction pattern was not represented in existing databases. Further investigation is needed to resolve this issue.

Table 2. Activation energies (kJ/mol) for different stages of crystallization in the amorphous Al–Ni–Co–Nd(Sm) alloys

Composition	E_1	E_2	E_3	E_4
$Al_{86}Ni_4Co_4Nd_6$	439	240	208	–
$Al_{86}Ni_4Co_4Sm_6$	408	351	273	–
$Al_{86}Ni_6Co_2Nd_6$	353	339	216	–
$Al_{86}Ni_6Co_2Sm_6$	262	454	239	259

Thus, the crystallization onset temperatures and activation energies obtained here provide conclusive evidence that the $Al_{86}Ni_4Co_4Nd_6$ alloy has a broader stability range of its amorphous phase and is more thermally stable in comparison with the samarium-containing alloy. The 4% Ni + 4% Co combination is preferable to the 6% Ni + 2% Co combination for amorphous phase stabilization.

Figure 7 shows typical resistivity curves of the $Al_{86}Ni_4Co_4Sm_6$ and $Al_{86}Ni_6Co_2Sm_6$ alloys and a previously studied $Al_{86}Ni_8Sm_6$ sample [8].

The resistivity of the amorphous alloys was found to be rather high, at a level of 120 μΩ cm. It is a weak function of temperature and has a negative temperature coefficient for all of the alloys. During crystallization, the resistivity decreases by more than a factor of 2,

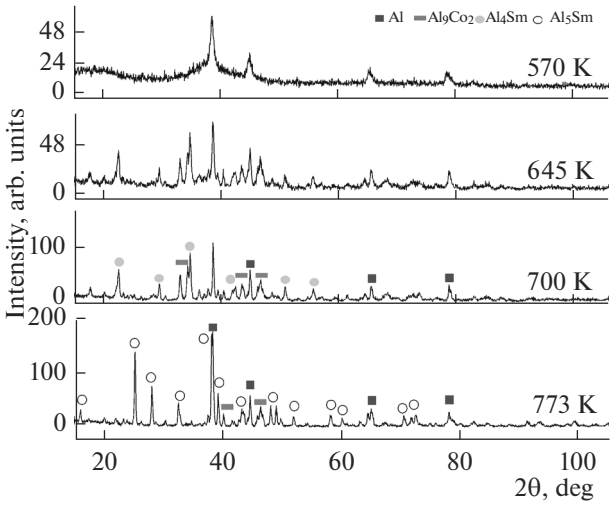

Fig. 5. X-ray diffraction patterns of the $Al_{86}Ni_6Co_2Sm_6$ sample.

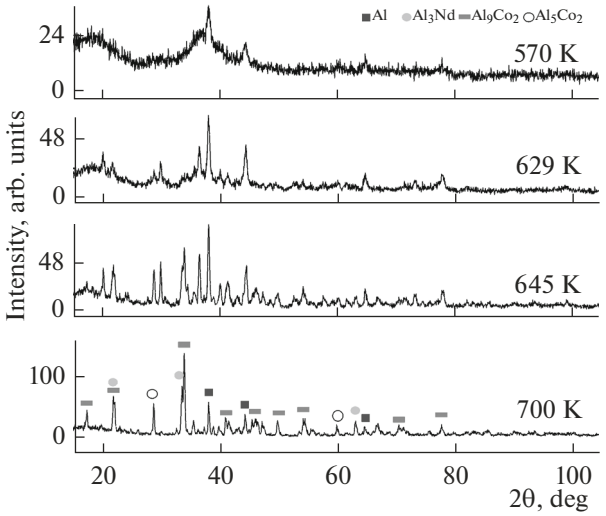

Fig. 6. X-ray diffraction patterns of the $Al_{86}Ni_4Co_4Nd_6$ sample.

passing through three stages (their temperatures are identical to those evaluated from the DSC data to within ±3 K). It should be emphasized that, in the case of the samarium-containing ribbons, replacing 8 at % Ni by 6 at % Ni + 2 at % Co extends the temperature range of the amorphous state by 30 K (T_{x1} shifts from 439 to 468 K). Further increasing the amount of Co to 4 at % extends the temperature range of the amorphous state by 100 K (T_{x1} shifts from 439 to 535 K). Note that anomalous $R(T)$ behavior was also observed at $T \simeq 730$ K.

Resistivity curves of the neodymium-containing alloy with 4 at % Ni and 4 at % Co have a number of distinctive features as compared to the samarium-containing alloy. The second stage of the decrease in resistivity during crystallization occurs in a wide temperature range (the resistivity gradually decreases with increasing T), whereas the third stage is represented by a small segment of the curve compared to the second stage. Above 650 K, the resistivity rises linearly with increasing temperature. No anomalies were detected near 730 K.

The anomalous $R(T)$ behavior around 730 K in the case of the samarium-containing alloys is attributable to the cubic-to-rhombohedral phase transformation of the intermetallic compound Al_3R. Such polymorphic transformations are typically not accompanied by considerable heat effects, but show up in temperature dependences of electron-sensitive properties [16].

The observed decrease in resistivity with increasing temperature for the amorphous phase can be accounted for as follows: Heating of amorphous Al–TM–REM alloys is known to cause phase separation well below the crystallization temperature. The effect was discovered by Gangopadhyay et al. [17] and was later confirmed many times for a variety of alloys (see, for example, Radiguet et al. [18] and Abrosimova et al. [19]). The formation of low-resistivity microregions consisting of essentially pure aluminum, whose size considerably exceeds interatomic distances, in a disordered amorphous matrix leads to a reduction in the total resistivity of the alloy. The larger the volume fraction of such microregions, the lower the resistivity of the material. When the crystallization of the ribbon reaches completion, its resistivity passes through a minimum and then begins to rise with increasing temperature, which is characteristic of crystalline alloys. This issue was addressed in detail previously [8].

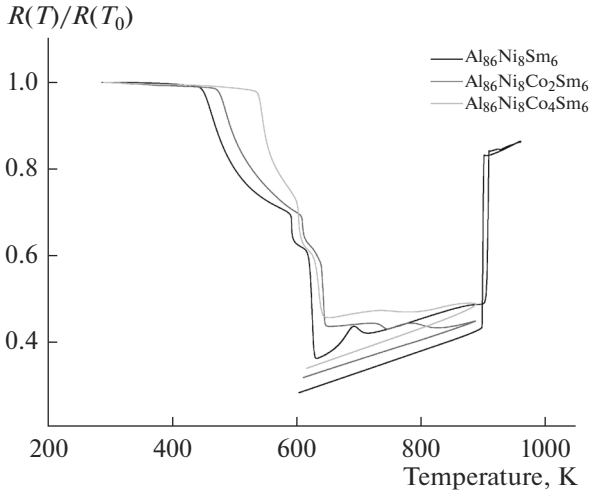

Fig. 7. Relative resistivity curves of the $Al_{86}Ni_8Sm_6$ [8], $Al_{86}Ni_4Co_4Sm_6$, and $Al_{86}Ni_6Co_2Sm_6$ alloys.

Thus, the present resistivity data confirm that the neodymium-containing amorphous alloys are more thermally stable than the samarium-containing alloys and that the 4% Ni + 4% Co combination is more preferable than the 6% Ni + 2% Co combination for amorphous phase stabilization.

CONCLUSIONS

The present DSC and resistivity data demonstrate that the amorphous Al–Ni–Co–Nd(Sm) alloys have a broader temperature range of an amorphous state (by 100 K) than do Ni- or Co-containing ternary alloys and exhibit more complex crystallization behavior. Neodymium is more preferable than samarium for improving the glass-forming ability of these alloys, and the 4% Ni + 4% Co combination is better than 6% Ni + 2% Co.

ACKNOWLEDGEMENT

This work was supported by the projects VEGA 2/0082/17 and APVV-15-0049. B. Rusanov gratefully acknowledges the fellowship of the Slovak Academic Information Agency (SAIA).

REFERENCES

1. Inoue, A., Ohtera, K., Tsai, A.P., and Masumoto, T., Aluminum-based amorphous alloys with tensile strength above 980 MPa (100 kg/mm^2), *Jpn. J. Appl. Phys.,* 1988, vol. 27, pp. L479–L482.

2. Gloriant, T. and Greer, A.L., Al-based nanocrystalline composites by rapid solidification of Al–Ni–Sm alloys, *Nanostruct. Mater.,* 1998, vol. 10, pp. 389–396. https://doi.org/10.1016/S0965-9773(98)00079-8

3. Triveco Rios, C., Suricach, S., Bary, M.S., et al., Glass forming ability of the Al–Ce–Ni system, *J. Non-Cryst. Solids,* 2008, vol. 354, pp. 4874–4877.

4. Ouyang, Y., Zhang, J., Chen, H., Liao, S., and Zhong, X., Crystallization study of amorphous $Al_{82}Fe_5Ni_5Ce_8$ alloy, *J. Alloys Compd.,* 2008, vol. 454, pp. 359–363.

5. Botta, W.J., Triveno Rios, C., SaLisboa, R.D., et al., Crystallization behaviors of Al-based metallic glasses: compositional and topological aspects, *J. Alloys Compd.,* 2009, vol. 483, pp. 89–93.

6. Li, C.L., Wang, P., Sun, S.Q., Voisey, K.T., and McCartney, D.G., Corrosion behaviour of $Al_{86.0}Co_{7.6}Ce_{6.4}$ glass forming alloy with different microstructures, *Appl. Surf. Sci.,* 2016, vol. 384, pp. 116–124. https://doi.org/10.1016/j.apsusc.2016.04.188

7. Vlasak, G., Duhaj, P., Patrasova, H., and Svec, P., Apparatus for thermal dilatation and magnetostriction measurements of amorphous ribbons, *J. Phys. E, Sci. Instrum.,* 1983, vol. 16, pp. 1203–1207.

8. Sidorov, V., Svec, P., Svec, P., Sr., Janickovic, D., Mikhailov, V., Sidorova, E., and Son, L., Electric and magnetic properties of $Al_{86}Ni_8R_6$ (R = Sm, Gd, Ho) alloys in liquid and amorphous states, *J. Magn. Magn. Mater.,* 2016, vol. 408, pp. 35–40. https://doi.org/10.1016/j.jmmm.2016.02.021

9. Gich, M., Gloriant, T., Surinach, S., Greer, A.L., and Baro, M.D., Glass forming ability and crystallisation processes within the Al–Ni–Sm system, *J. Non-Cryst. Solids,* 2001, vol. 289, pp. 214–220. https://doi.org/10.1016/S0022-3093(01)00650-0

10. Illekova, E., Duhaj, P., Mrafko, P., and Svec, P., Influence of Pd on crystallization of Al–Ni–Sm-based ribbons, *J. Alloys Compd.,* 2009, vol. 483, pp. 20–23. https://doi.org/10.1016/j.jallcom.2008.08.106

11. Sun, F. and Gloriant, T., Primary crystallization process of amorphous $Al_{88}Ni_6Sm_6$ alloy investigated by differential scanning calorimetry and by electrical resistivity, *J. Alloys Compd.,* 2009, vol. 477, pp. 133–138. https://doi.org/10.1016/j.jallcom.2008.10.021

12. Zhang, Y., Warren, P.J., and Cerezo, A., Effect of Cu addition on nanocrystallisation of Al–Ni–Sm amorphous alloy, *Mater. Sci. Eng., A,* 2002, vol. 327, pp. 109–115. https://doi.org/10.1016/S0921-5093(01)01888-3

13. Gangopadhyay, A.K. and Kelton, K.F., Effect of rare-earth atomic radius on the devitrification of $Al_{88}RE_8Ni_4$ amorphous alloys, *Philos. Mag. A,* 2000, vol. 80, pp. 1193–1206. https://doi.org/10.1080/01418610008212110

14. Revesz, A., Varga, L.K., Nagy, P.M., Lendvai, J., and Bakonyi, I., Structure and thermal stability of melt-quenched $Al_{92-x}Ni_8(Ce,Sm)_x$ alloys with x = 1, 2 and 4, *Mater. Sci. Eng., A,* 2003, vol. 351, pp. 160–165. http://dx.doi.org/ 00823-7 https://doi.org/10.1016/S0921-5093(02)

15. Kissinger, H.E., Reaction kinetics in differential thermal analysis, *Anal. Chem.,* 1957, vol. 29, pp. 1702–1706.

16. Sidorov, V., Petrova, S., Svec, P., Sr., et al., Crystallization of Al–Co–Dy(Ho) amorphous alloys, *Eur. Phys. J. Spec. Top.,* 2017, vol. 226, pp. 1107–1113. https://doi.org/10.1140/epjst/e2016-60226-x

17. Gangopadhyay, A.K., Croat, T.K., and Kelton, K.F., The effect of phase separation on subsequent crystallization in $Al_{88}Gd_6La_2Ni_4$, *Acta Mater.,* 2000, vol. 48, pp. 4035–4043. https://doi.org/10.1016/S1359-6454(00)00196-8

18. Radiguet, B., Blavette, D., Wanderka, N., Banhart, J., and Sahoo, K.L., Segregation-controlled nanocrystallization in an Al–Ni–La metallic glass, *Appl. Phys. Lett.,* 2008, vol. 92, paper 103 126. https://doi.org/10.1063/1.2897303

19. Abrosimova, G., Aronin, A., and Budchenko, A., Amorphous phase decomposition in Al–Ni–RE system alloys, *Mater. Lett.,* 2015, vol. 139, pp. 194–196. https://doi.org/10.1016/j.matlet.2014.10.076